EUROPEAN ORGANIZATION FOR NUCLEAR RESEARCH

L3 Note 2383
March 15, 1999

Search for Neutral Higgs Bosons of the Minimal Supersymmetric Standard Model in e^+e^- Interactions at $\sqrt{s} = 189$ GeV

L3 Collaboration

Abstract

A search for the lightest neutral scalar and neutral pseudoscalar Higgs bosons in the Minimal Supersymmetric Standard Model is performed on 176.4 pb^{-1} of integrated luminosity collected by L3 at a center-of-mass energy of 189 GeV. No excess of events consistent with a signal is observed. Limits on the masses of the lightest neutral scalar and pseudoscalar are given as a function of $\tan\beta$. Lower mass limits independent of $\tan\beta$ are set at the 95% confidence level to be $m_{\mathrm{h}} > 77$ GeV and $m_{\mathrm{A}} > 78$ GeV.

Results reported in this note are PRELIMINARY:
They are submitted to the speakers of the 1999 Winter conferences.

1 Introduction

In the Standard Model [1], one Higgs doublet [2] is responsible for the introduction of one neutral, scalar particle, the Higgs boson. No such scalars have been observed and the previous published lower limit GeV [1)] on its mass has been set by L3 at 87.6 [3]; a preliminary analysis of the data at 189 GeV yields a lower limit of 95.2 GeV [4]. In contrast to the Standard Model, the Minimal Supersymmetric Standard Model [5] introduces two Higgs doublets, which give rise to a charged scalar pair, two neutral scalars, the lightest of which is called h, and a neutral CP-odd scalar, called A. We consider the two production mechanisms most important at LEP2 center-of-mass energies:

$$\mathrm{e^+e^-} \rightarrow \mathrm{Z^*} \rightarrow \mathrm{hZ} \tag{1}$$
$$\mathrm{e^+e^-} \rightarrow \mathrm{Z^*} \rightarrow \mathrm{hA}. \tag{2}$$

The rate for the Higgs-bremsstrahlung process (1) is usually smaller than the similar Standard Model reaction, but this is compensated by the additional pair-production process (2) [6].

The lower limit on m_h and m_A previously published by L3 on the $130 - 183$ GeV data was $m_\mathrm{h} > 70.7$ GeV and $m_\mathrm{A} > 71.0$ GeV [7]. This note briefly describes the analyses done on the data collected by L3 in 1998 at $\sqrt{s} = 189$ GeV and is meant as a guideline to speakers at the 1999 Winter conferences. **All results should be considered as preliminary.**

2 Data and Monte Carlo Samples

The data collected during 1998 by the L3 detector had an average center-of-mass energy of 189 GeV and an integrated luminosity of 176.4 pb^{-1}. During the 1998 run, 2.5 pb^{-1} of data at $\sqrt{s} = 91$ GeV was also taken for calibration purposes.

The signal cross sections and branching ratios are calculated using the HZHA generator [8]. For the efficiency studies, Monte Carlo samples of Higgs events are generated using PYTHIA [9]. For the background studies, the following Monte Carlo programs are used: PYTHIA ($\mathrm{e^+e^-} \rightarrow \mathrm{q\bar{q}}$), KORALW [10] ($\mathrm{e^+e^-} \rightarrow \mathrm{W^+W^-}$), KORALZ [11] ($\mathrm{e^+e^-} \rightarrow \tau^+\tau^-$), PYTHIA and PHOJET [12] ($\mathrm{e^+e^-} \rightarrow \mathrm{e^+e^-q\bar{q}}$), and EXCALIBUR [13] ($\mathrm{e^+e^-} \rightarrow \mathrm{f\bar{f}'f\bar{f}'}$). These are the same backgrounds used in the Standard Model Higgs search [4] and the number of simulated events for the most important backgrounds is reproduced from Reference [4] in Table 1.

SM processes	cross section (pb)	Generator	Events
$\mathrm{e^+e^-} \rightarrow \mathrm{e^+e^-q\bar{q}}$ ($\mathrm{M_{q\bar{q}}} > 15$ GeV)	4.11×10^3	PHOJET	2×10^6
$\mathrm{e^+e^-} \rightarrow \mathrm{q\bar{q}}$	98.3	PYTHIA	2.93×10^6
$\mathrm{e^+e^-} \rightarrow \mathrm{W^+W^-}$ (except $\mathrm{q\bar{q}'e}\nu$)	14.1	KORALW	2.5×10^5
$\mathrm{e^+e^-} \rightarrow \mathrm{Ze^+e^-}$	3.35	PYTHIA	3×10^4
$\mathrm{e^+e^-} \rightarrow \mathrm{q\bar{q}'e}\nu$	2.9	EXCALIBUR	7.9×10^3
$\mathrm{e^+e^-} \rightarrow \mathrm{ZZ}$	0.973	PYTHIA	1.96×10^5

Table 1: Standard Model processes, cross sections, generators, and number of MC events at $\sqrt{s} = 189$ GeV, used in the analyses.

[1)] Unless otherwise stated, the mass limits discussed in this note are at the 95% confidence level.

3 Analysis Procedures

The search for hA and hZ production is carried out using one set of Minimal Supersymmetric Standard Model parameters similar to those used in the previous searches by L3 [7]. The set of parameters used here is called "maximal mixing" and corresponds to particular values of the parameters assumed to be free: the ratio of the two Higgs vacuum expectation values, $\tan\beta$; the pseudoscalar Higgs mass, m_{A}; the gaugino mass parameter, M_2; the scalar fermion mass, m_0; the scalar quark mixing mass, A; and the Higgs mass parameter, μ. The maximal mixing set corresponds to $A = \sqrt{6}$ TeV, $\mu = -0.1$ TeV, $M_2 = m_0 = 1$ TeV and the mass of the top quark, m_{t}, is taken to be $m_{\mathrm{t}} = 175$ GeV [14]. Finally, a scan over the two remaining independent parameters, $\tan\beta$ and m_{A}, is performed for the ranges

$$1 \leq \tan\beta \leq 50$$
$$30 \text{ GeV} \leq m_{\mathrm{A}} \leq 1000 \text{ GeV} .$$

Other benchmark mixing scenarios and values of $\tan\beta$ and m_{A} outside of these ranges are not considered in this note, but will be included in future studies.

Because the relative rates of the complementary processes, $\mathrm{e^+e^-} \rightarrow \mathrm{Z^*} \rightarrow \mathrm{hA}$ and $\mathrm{e^+e^-} \rightarrow \mathrm{Z^*} \rightarrow \mathrm{hZ}$, varies over the range of parameters considered, it is important to carry out an analysis that has good sensitivity to both channels for a broad range of these parameters. Four event topologies representing $\sim 98\%$ of the decay modes of hZ decay are considered: $\mathrm{q\bar{q}q\bar{q}}$, $\mathrm{q\bar{q}}\nu\bar{\nu}$, $\mathrm{q\bar{q}}\ell^+\ell^-$ ($\ell = \mathrm{e}, \mu, \tau$) and $\tau^+\tau^-\mathrm{q\bar{q}}$. The analyses of the $\mathrm{q\bar{q}}\nu\bar{\nu}$ and $\mathrm{q\bar{q}}\ell^+\ell^-$ ($\ell = \mathrm{e}, \mu$) channels were taken from the Standard Model Higgs search [4]. The hZ analyses are optimized for $\mathrm{h} \rightarrow \mathrm{b\bar{b}}$, but the efficiencies for the small contributions from the decay modes $\mathrm{h} \rightarrow \mathrm{c\bar{c}}, \mathrm{gg}$ are also considered as well as small contributions from the $\mathrm{W^+W^-}$ and ZZ fusion processes, $\mathrm{e^+e^-} \rightarrow \mathrm{h}\nu\bar{\nu}$ and $\mathrm{e^+e^-} \rightarrow \mathrm{he^+e^-}$.

Two event topologies for hA decay, which generally make up $\sim 97\%$ of the available decay modes[2)], are considered: $\mathrm{hA} \rightarrow \mathrm{b\bar{b}b\bar{b}}$ and $\mathrm{hA} \rightarrow \mathrm{b\bar{b}}\tau^+\tau^-$ ($\tau^+\tau^-\ \mathrm{b\bar{b}}$). These topologies are quite similar to their hZ counterparts, but the Z-mass constraint cannot be used and, on average, the hA events are more likely to contain b hadrons.

Both the hZ and hA analyses are performed in three stages. First, a high multiplicity hadronic event selection is applied, which greatly reduces the data set by almost eliminating the huge contribution from two-photon processes (see top row of Table 1), but which also maintains a high signal efficiency above 95%. Second, selection criteria optimized for the particular topology in question are applied. These cuts are chosen using an automated procedure and still allow for a high signal efficiency and many candidates. Third, a final, discriminating variable is built which depends on the mass hypothesis and the relative rates of hA and hZ production. In this way, each point in the scan over $\tan\beta$ and m_{A} represents a separate optimized analysis. **The full spectrum of the discriminating variable is then used to calculate the confidence level that the data are consistent with a Higgs signal.**

The b-tagging variable [15, 16] plays a large role in the calculation of this discriminant due to the high expected branching fraction of Higgs particles into b quarks. A neural network output for each hadronic jet is calculated from inputs including the measured decay lengths of particles in three dimensions, information about prompt leptons and jet shape variables. The event b-tag variable, $B_{\mathrm{tag}}^{\mathrm{event}}$, is then defined to be the negative-logarithm of the probability that all the hadronic jets in the event are consistent with jets containing no b hadrons. The

[2)]For these ranges of Minimal Supersymmetric Standard Model parameters.

performance of this event tag is shown in Figure 1 on the data collected at $\sqrt{s} = 91$ GeV at the beginning of the 1998 run.

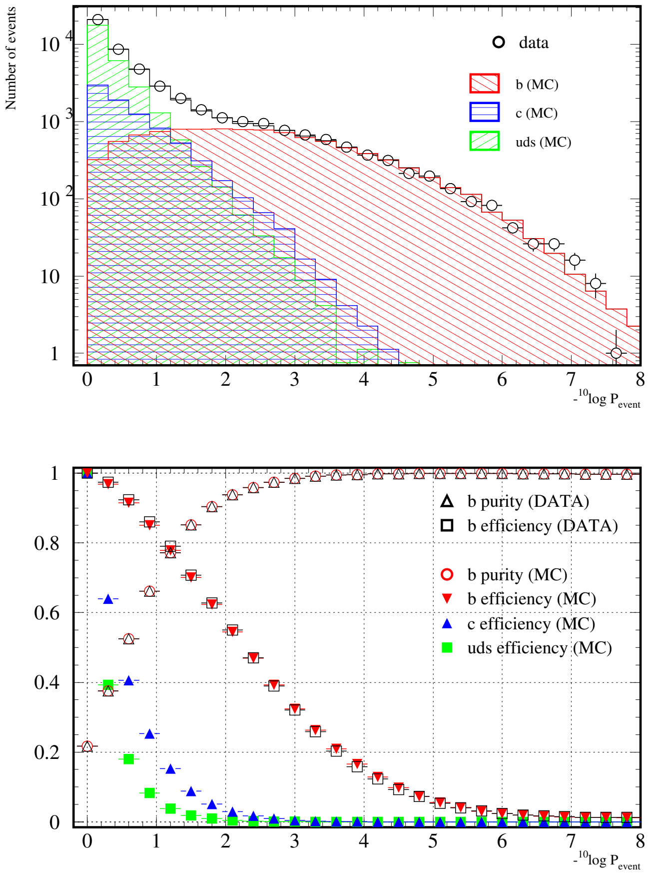

Figure 1: Neural network b-tag in 1998 on Z-peak data. The jet-tags are combined into an event tag which is shown for $|\cos\theta_{\rm thrust}| < 0.72$.

4 Four-Jets Channels

The signature of the $\mathrm{hA \rightarrow b\bar{b}b\bar{b}}$ and $\mathrm{hZ \rightarrow b\bar{b}q\bar{q}}$ decay modes is four high-multiplicity hadronic jets and the presence of b hadron decay products. The dominant backgrounds come from $\mathrm{q\bar{q}}$ production, hadronic decays of W-pairs and an especially difficult contribution comes from ZZ decays containing b quarks. In the case of $\mathrm{hA \rightarrow b\bar{b}b\bar{b}}$, the identification of b hadrons plays a particularly important role. Both analyses proceed in three stages.

First, a high-multiplicity hadronic event preselection common to both channels is made at all center-of-mass energies. At least 15 tracks and 20 calorimetric clusters are required; the visible energy, $E_{\rm vis}$, must exceed $0.6\sqrt{s}$; the event must be balanced having not more than 30% of the missing energy parallel or perpendicular to the beam direction; radiative returns to the Z-resonance are rejected with a maximum lepton or photon energy cut of 65 GeV. Finally, a loose cut of $Y_{34}^{\rm D} > 0.0025$ parameter[3)] in the DURHAM [17] scheme rejects a large number of two-jet events. Events passing the preselection are then forced to have four jets using the

[3)] $Y_{34}^{\rm D}$ is the $Y_{\rm cut}$ in the DURHAM scheme where the event goes from having three to four jets.

DURHAM clustering algorithm and a kinematic fit requiring 4-momentum conservation (4C) is performed.

The second stage of the analyses optimizes the signal sensitivity by automatically adjusting a set of cuts to maximize the average confidence level calculated only from Monte Carlo signal and background expectations using the technique described in References [15,18]. The cuts are optimized on the following variables:

- $\boldsymbol{B_{\mathrm{tag}}^{\mathrm{event}}}$: A loose cut on the b-tag is capable of removing a large portion of the $\mathrm{W^+W^-}$ background. A tight cut is not made since the entire $B_{\mathrm{tag}}^{\mathrm{event}}$ spectrum will be combined with the mass information in the construction of the final, discriminating variable.

- **Mass variable**: The following mass χ^2 variable is defined separately for $\mathrm{hZ \rightarrow b\bar{b}q\bar{q}}$ and $\mathrm{hA \rightarrow b\bar{b}b\bar{b}}$:

$$\chi^2(m_{\mathrm{X}}, m_{\mathrm{h}}) = \min\left((\Sigma_i - (m_{\mathrm{X}} + m_{\mathrm{h}}))^2 w_\Sigma + (\Delta_i - |m_{\mathrm{X}} - m_{\mathrm{h}}|)^2 w_\Delta\right) , \tag{3}$$

  where m_{X} is either m_{Z} or m_{A}, depending on the test performed. The index i runs over the three possible dijet pairings, Σ_i and Δ_i are the sum and difference of the dijet masses of the i^{th} dijet pair, (m_i, m_i'). The weights, w_Σ and w_Δ, are respectively $1/(4\ \mathrm{GeV})^2$ and $1/(6\ \mathrm{GeV})^2$, reflecting the typical mass resolutions. This mass χ^2 runs over many orders of magnitude making it difficult to use in a computer program. Therefore, we define the mass variable to be the logarithm of the probability of the mass χ^2 for two degrees of freedom

$$\chi_{\mathrm{hZ}} = \log P\left(\chi^2(m_{\mathrm{Z}}, m_{\mathrm{h}})\right) \tag{4}$$
$$\chi_{\mathrm{hA}} = \log P\left(\chi^2(m_{\mathrm{A}}, m_{\mathrm{h}})\right) . \tag{5}$$

- $\boldsymbol{Y_{34}^{\mathrm{D}}}$: This variable is somewhat sensitive to how close the hypothesized Higgs mass is to the kinematic limit. Cuts larger than 0.008 are strong four-jet requirements, while cuts around 0.002 select more three-jet-like events but are very efficient at selecting four-jet events.

- $\boldsymbol{\max(\Delta E_{\mathrm{jet}})}$: The maximum energy difference between any two jets. Typical values of this cut require $\max(\Delta E_{\mathrm{jet}})$ to be less than about 35% of the center-of-mass energy. This is meant to reject soft gluon jets which frequently occur in $\mathrm{e^+e^-} \rightarrow \mathrm{Z}^*/\gamma^* \rightarrow \mathrm{q\bar{q}}$ events which have four or more jets.

- $\boldsymbol{\min(E_{\mathrm{jet}})}$: The minimum jet energy. This is strongly related to the cut on $\max(\Delta E_{\mathrm{jet}})$, but a cut of $\sim 8\%\sqrt{s}$ kills events with four low energy jets which otherwise would slip by. This is a fairly weak cut.

- $\boldsymbol{m_i}$: The minimum and maximum dijet mass. For all three combinations of jets which give pairs of dijet masses, (m_i, m_i'), both m_i and m_i' are required to be within a certain range. Actually, both the lower and upper bound tend to remove soft gluonic jets since two jets with small opening angles can give large or small invariant masses depending on how they are paired. The optimum window usually has lower and upper bounds of 10% and 80% of the center-of-mass energy.

- $\boldsymbol{N_{\mathrm{trk}}}$: The number of tracks passing some quality cuts is also optimized since the signal has a higher multiplicity than much of the background.

These cuts are optimized at two points in the $(\tan\beta, m_{\rm A})$ plane: 1) for the hZ channel with $m_{\rm h} = 97$ GeV; 2) and for the hA channel at high $\tan\beta$ with $m_{\rm A} = m_{\rm h} = 80$ GeV. The results of the optimization can be found in Table 2 and plots of the four most important of these variables can be found in Figure 2 at the preselection level. The b-tag and mass cuts are not applied at this level but after making a unique assignment to either the $\mathrm{hA \to b\bar{b}b\bar{b}}$ or $\mathrm{hZ \to b\bar{b}q\bar{q}}$ hypothesis. The effect of the preselection and optimized cuts on the expected background, signal and observed data is listed in Table 3 (compare to background cross sections in Table 1).

Channel	$Y_{34}^{\rm D}$	$\max(\Delta E_{\rm jet})$	$\min(E_{\rm jet})$	$\min(m_i)$	$\max(m_i)$	$N_{\rm trk}$
hZ	> 0.0105	< 0.255	> 0.137	> 0.145	< 0.628	> 21
hA	> 0.0034	< 0.292	> 0.106	> 0.097	< 0.731	> 24

Table 2: Optimized cuts in the four-jets analyses.

	(events or % efficiency)		
Process	Preselection	hA cuts	hZ cuts
$\mathrm{e^+e^- \to e^+e^-q\bar{q}}$	44.0	4.2	0.5
$\mathrm{e^+e^- \to q\bar{q}}$	1076.0	239.1	84.4
$\mathrm{e^+e^- \to W^+W^-}$	1417.0	944.5	605.3
$\mathrm{e^+e^- \to q\bar{q}'e\nu}$	52.6	3.5	1.5
$\mathrm{e^+e^- \to ZZ}$	84.4	50.8	39.1
Total	2674.0	1242.0	730.8
Data	2627	1164	679
$\mathrm{hA \to b\bar{b}b\bar{b}}$	94.3%	76.3%	44.7%
$\mathrm{hZ \to b\bar{b}q\bar{q}}$	96.4%	78.3%	63.8%

Table 3: Analysis flow in the four-jets channels. The signal efficiencies are quoted for $m_{\rm A} = m_{\rm h} = 80$ GeV and $m_{\rm h} = 97$ GeV.

Events passing the optimized cuts are then classified into three categories: 1) those that pass only the hA cuts; 2) those that pass only the hZ cuts[4)]; and 3) those that pass both sets of cuts. Category (1) is called the $\mathrm{hA_{b\bar{b}b\bar{b}}}$ analysis and category (2) is called the $\mathrm{hZ_{b\bar{b}q\bar{q}}}$ analysis. Category (3) is then split into two separate samples by choosing the most likely production hypothesis based on the probability of the χ^2 of the mass hypothesis and the relative production rates of hA and hZ. If the hZ hypothesis is more likely, then the event is classified as $\mathrm{hZ'_{b\bar{b}q\bar{q}}}$, otherwise it is called $\mathrm{hA'_{b\bar{b}b\bar{b}}}$.

In the last stage of the four-jets analyses, a weighted combination of the probabilities that the $B_{\rm tag}^{\rm event}$ and χ values for the event are consistent with their background distributions is made using the technique described in Reference [7]. The relative weight in the probability combination as well as the cuts on the b-tag and mass variables are optimized for each of the four sub-categories. The spectrum of this discriminating variable is remade at each point in the $(\tan\beta, m_{\rm A})$ scan as the mass hypothesis changes. This is done for each of the four-jets sub-analyses, $\mathrm{hZ_{b\bar{b}q\bar{q}}}$, $\mathrm{hA_{b\bar{b}b\bar{b}}}$, $\mathrm{hZ'_{b\bar{b}q\bar{q}}}$ and $\mathrm{hA'_{b\bar{b}b\bar{b}}}$, at each scanned point as well since the analysis

[4)] The hZ cuts are almost a subset of the hA cuts.

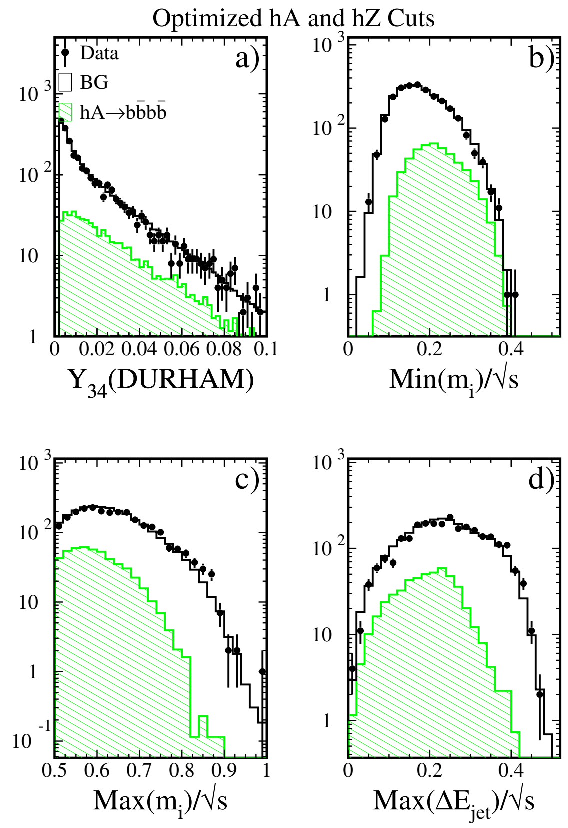

Figure 2: Variables used in the cut optimizer for the four-jets analyses after preselection.

splitting depends on the relative rates of hZ and hA production. The spectrum of the final variable is shown in Figure 3 for each of the three sub-analysis types.

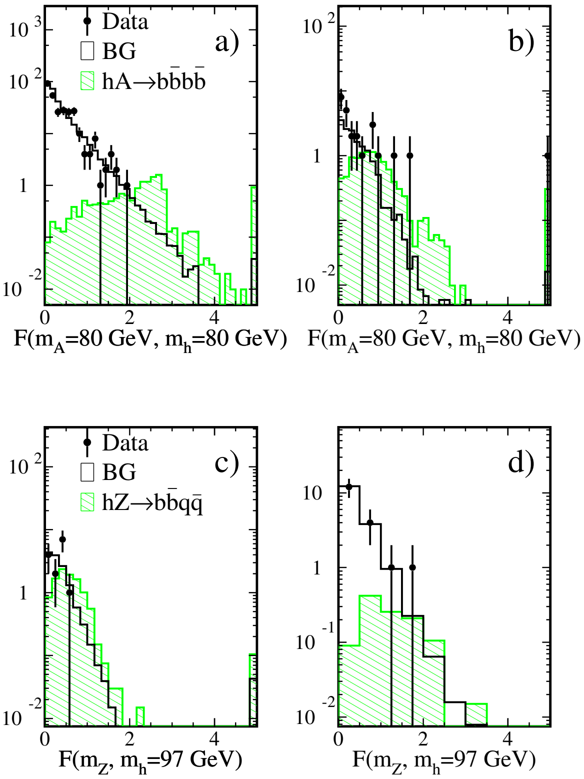

Figure 3: Final, discriminating variable for a) $\mathrm{hA}'_{\mathrm{b\bar{b}b\bar{b}}}$, b) $\mathrm{hA}_{\mathrm{b\bar{b}b\bar{b}}}$, c) $\mathrm{hZ}'_{\mathrm{b\bar{b}q\bar{q}}}$ and d) $\mathrm{hZ}_{\mathrm{b\bar{b}q\bar{q}}}$ four-jets sub-analyses, with $m_{\mathrm{A}} = m_{\mathrm{h}} = 80$ GeV and $m_{\mathrm{h}} = 97$ GeV.

5 Tau Channels

The signatures of $hA \to b\bar{b}\tau^+\tau^-(\tau^+\tau^- b\bar{b})$, $hZ \to b\bar{b}\tau^+\tau^-$ or $hZ \to \tau^+\tau^- q\bar{q}$ events are a pair of high-energy taus accompanied by two hadronic jets. The main background comes from W-pair decays containing taus. Two analyses are optimized for the hZ and for the hA channels. The hZ analysis is described in detail in reference [4]. We will describe here only the $hA \to b\bar{b}\tau^+\tau^-(\tau^+\tau^- b\bar{b})$ selection[5)]. Two selections are performed, one based on the τ identification (particle based selection) and one relying more on the event kinematics (jet based selection).

First, a common preselection is applied, requiring more than 8 charged tracks, more than 14 clusters and a visible energy of more than $0.4\sqrt{s}$. The events are subject to the DURHAM algorithm with $\log Y_{34}^{\mathrm{D}} \geq -6$, Y_{34}^{D} being the same jet parameter used in the four-jets analysis in Section 4. Background from $q\bar{q}(\gamma)$ events is reduced by rejecting events with photons of more than 20 GeV. The contribution of $W^+W^- \to q\bar{q}\ell\nu, \ell = e, \mu$ is reduced by requiring the energy of electrons and muons to be smaller than 45 GeV.

In the particle based selection tau leptons are identified via their decay into electrons or muons or as an isolated low-multiplicity jet with 1 or 3 tracks and unit charge. In the jet based selection the event is forced into four jets using the DURHAM algorithm. Two of the jets must have less than 4 tracks. These jets are considered as tau candidates. At least one of these tau candidates must coincide with a tau candidate defined in the particle based selection within 3°. Both taus must be separated from the hadronic jets by at least 25°. For both selections the missing momentum vector is transformed into the rest frame of the particle decaying into the taus. In this frame the missing momentum vector is relatively mass independent and must be smaller than 40 GeV. This cut rejects $W^+W^- \to q\bar{q}\ell\nu, (\ell = e, \mu, \tau)$ events and allows sensitivity over a wide mass range. The visible energy is required to be smaller than $0.9\sqrt{s}$ for the particle based and smaller than $0.85\sqrt{s}$ for the jet based selection to reject $W^+W^- \to q\bar{q}$ events.

For the jet based selection we require in addition that the visible mass is smaller than 175 GeV and that the missing momentum vector satisfies $|\cos\theta_{\mathrm{miss}}| \leq 0.9$. As both the h and the A are scalars, the production follows a $\sin^2\theta$ dependence whereas the major fraction of the background is collected in the forward-backward region of the detector. The production angle must satisfy $|\cos\theta| \leq 0.85$. Furthermore, we require that the ratio of the sum of the decay products of the taus and the sum of the jet energies must be smaller than 1. In the jet based selection the opening angle between the taus must be at least 40° and between the hadronic jets at least 50°. A kinematic fit is performed requiring energy and momentum conservation. The directions of the jets and of the tau decay products are kept at their measured values. Events are accepted if the jet-jet and the tau-tau masses after the fit are in the range between 25 GeV and 100 GeV. Table 4 summarizes the number of observed candidates, the expected background from Standard Model processes and the signal efficiencies.

For the final variable (which is used for the limit calculation) we combine the b-tag information with the reconstructed tau-tau and jet-jet masses obtained from the kinematic fit in the following way: For each event class j $(ZZ, W^+W^-, q\bar{q}, hA)$, a probability density function f_i^j is constructed, where i denotes the tau-tau mass, the jet-jet mass, b-tag$_1$ or b-tag$_2$ (jet tags).

[5)] From now on, it will be understood that the so-called $hA \to b\bar{b}\tau^+\tau^-$ analysis also includes the charge-conjugate mode, even if it is not specifically mentioned.

The probability for variable i to belong to the event class j is then defined as:

$$\mathrm{p}_\mathrm{i}^\mathrm{j} = \frac{\mathrm{f}_\mathrm{i}^\mathrm{j}}{\sum_\mathrm{k} \mathrm{f}_\mathrm{i}^\mathrm{k}} \tag{6}$$

and the likelihood for an event to belong to the signal class hA is:

$$\mathrm{F}^\mathrm{hA} = \frac{\prod_\mathrm{i} \mathrm{p}_\mathrm{i}^\mathrm{hA}}{\sum_\mathrm{k} \prod_\mathrm{i} \mathrm{p}_\mathrm{i}^\mathrm{k}} \tag{7}$$

Events, which pass the hA as well as the hZ selection are classified as either hA or hZ depending on the cross section weighted values of F^hA and F^hZ.

Process	events or % efficiency
$e^+e^- \to e^+e^- q\bar{q}$	1.8
$e^+e^- \to W^+W^-$	15.9
$e^+e^- \to ZZ$	3.9
Total	21.6
Data	20
$hA \to b\bar{b}\tau^+\tau^-$	39.8
$hZ \to b\bar{b}\tau^+\tau^-$	30.5
$hZ \to \tau^+\tau^- q\bar{q}$	32.5

Table 4: Selected candidates and background expectation for the tau channels. The signal efficiencies are quoted for $m_\mathrm{A} = m_\mathrm{h} = 80$ GeV and $m_\mathrm{h} = 97$ GeV. The events have passed either the hZ or the hA selection.

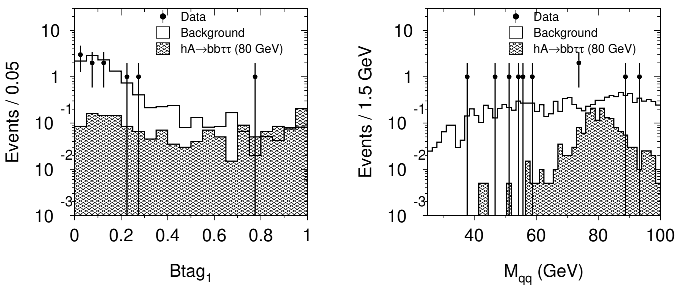

Figure 4: B-tag variable of the first jet and reconstructed jet-jet mass after the kinematic fit for the $hA \to b\bar{b}\tau^+\tau^-$ analysis. The events have passed either the particle or the jet based selection.

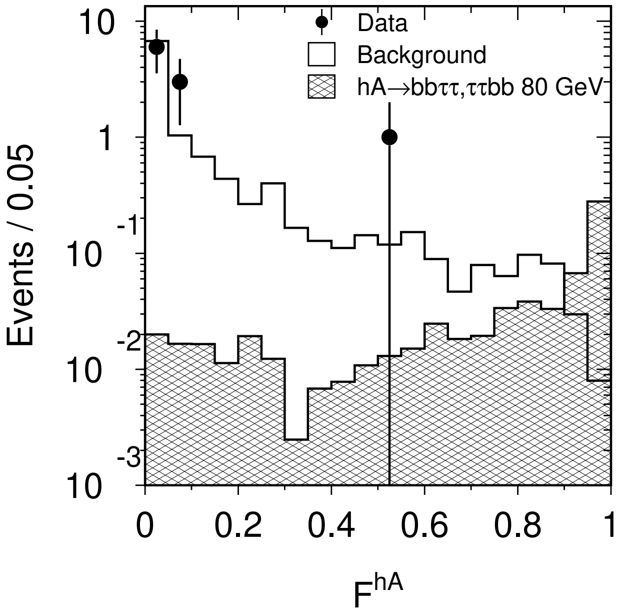

Figure 5: Final, discriminating variable for tau analyses at $m_{\mathrm{h}} = 80$ GeV and $\tan\beta = 50$.

6 Combination of Results & Mass Limits

No evidence of the production of the h and A bosons is observed in the data. The mass limits are evaluated by calculating the confidence level (CL) that the expected signal is absent in the observed data for the plane defined by $(\tan\beta, m_{\rm A})$ and, equivalently, in terms of $\tan\beta$ and $m_{\rm h}$. The CL is calculated using the technique described in References [19, 20]. The spectra of the final, discriminating variables of the analyses for all the physics processes and decay channels are combined into bins of one distribution, ordered in the logarithm of signal-over-background. The CL is then calculated from this signal-over-background distribution for each scanned point.

Lower limits on the mass of the lightest scalar, $m_{\rm h}$, as a function of $\tan\beta$ are shown in Figure 6 for the maximal mixing hypothesis. The results of the previous Higgs searches by L3 at center-of-mass energies less than 189 GeV [7, 21] is also included. For the MSSM parameters considered, this results in lower mass limits at the 95% CL of

$$m_{\rm h} > 77 \text{ GeV}, \quad m_{\rm A} > 78 \text{ GeV}.$$

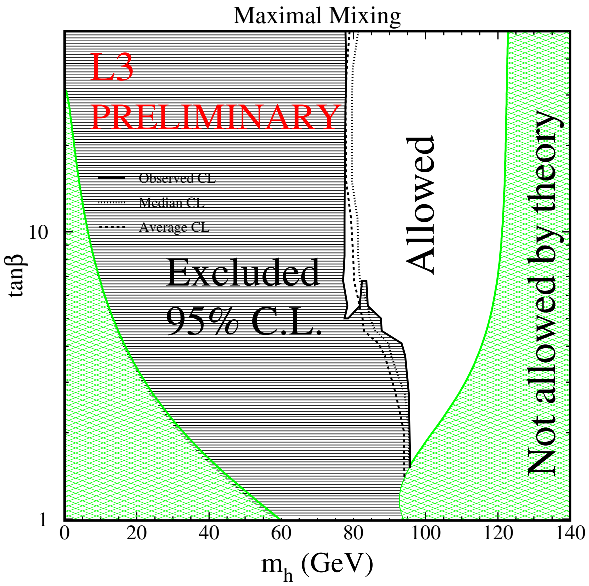

Figure 6: Exclusion plot of the Higgs mass, $m_{\rm h}$, vs. $\tan\beta$. Shown are the 95% observed and average exclusions. These limits include the results from previous searches up to $\sqrt{s} = 183$ GeV.

Acknowledgments

The authors would like to thank Peter Bock for the kind permission of using his general interpolation routines.

References

[1] S. L. Glashow, Nucl. Phys. **22** (1961) 579; S. Weinberg, Phys. Rev. Lett. **19** (1967) 1264; A. Salam, in Elementary Particle Theory, ed. N. Svartholm, (Almqvist and Wiksell, Stockholm, 1968), p. 367.

[2] P. W. Higgs, Phys. Lett. **12** (1964) 132; F. Englert and R. Brout, Phys. Rev. Lett. **13** (1964) 321; G. S. Guralnik *et al.*, Phys. Rev. Lett. **13** (1964) 585.

[3] M. Acciarri and others, Phys. Lett. **B 431** (1998) 437.

[4] L3 Higgs Working Group, "Standard Model Higgs Searches at $\sqrt{s} = 189$ GeV", L3 Internal note 2382, 1999.

[5] H. P. Nilles, Phys. Rep. **110** (1984) 1; H. E. Haber and G. L. Kane, Phys. Rep. **117** (1985) 75; R. Barbieri, Riv. Nuovo Cim. **11 n°4** (1988) 1.

[6] John F. Gunion and Howard E. Haber and Gordon Kane and Sally Dawson, The Higgs Hunter's Guide, (Addison Wesley, 1990).

[7] M. Acciarri and others, Phys. Lett. **B 436** (1998) 389.

[8] P. Janot, (CERN, Geneva, Switzerland, 1996), p. 309.

[9] T. Sjöstrand, "PYTHIA", Preprint TH/93-7112, CERN, 1993, Revised August 1995; T. Sjöstrand, Comp. Phys. Comm. **82** (1994) 74.

[10] M. Skrzypek and others, Comp. Phys. Comm. **94** (1996) 216; M. Skrzypek and others, Phys. Lett. **B 372** (1996) 289.

[11] S. Jadach and B. F. L. Ward and Z. Wąs, Comp. Phys. Comm. **66** (1991) 276.

[12] R. Engel, Z. Phys. **C 66** (1995) 203; R. Engel and J. Ranft and S. Roesler, Phys. Rev. **D 52** (1995) 1459.

[13] F. A. Berends and R. Pittau and R. Kleiss, Comp. Phys. Comm. **85** (1995) 437.

[14] CDF Collaboration, F. Abe and others, Phys. Rev. Lett. **80** (1998) 2767; D0 Collaboration, S. Abachi and others, Phys. Rev. Lett. **79** (1997) 1197.

[15] A. Dominguez, "Search for Neutral Higgs Bosons in e^+e^- Interactions at Center-of-Mass Energies Between 130 GeV and 183 GeV", Ph.D. thesis, UCSD, 1998, `http://hep.ucsd.edu/thesis/aaron.html`.

[16] J. Branson and A. Dominguez and I. Fisk and G. Raven, "The UCSD B Tag for 1996", L3 Internal note 2108, 1997.

[17] S. Bethke and others, Nucl. Phys. **B 370** (1992) 310.

[18] M. Biasini and others, "Standard Model Higgs searches at $\sqrt{s} = 183$ GeV", L3 Internal Note 2241, 1998.

[19] M. Acciarri and others, Phys. Lett. **B 411** (1997) 373.

[20] A. Favara and M. Pieri, “Confidence Level Estimation and Analysis Optimization”, L3 Internal Note 2066, 1997.

[21] O. Adriani and others, Z. Phys. **C 57** (1993) 355.